Adsorption (2007) 13: 407–424
DOI 10.1007/s10450-007-9026-4

On the physical adsorption of gases on carbon materials from molecular simulation

G.R. Birkett · D.D. Do

Received: 11 May 2007 / Revised: 9 July 2007 / Accepted: 13 July 2007 / Published online: 25 September 2007

Abstract In this paper we present a series of work covering a range of aspects relating molecular simulation to experiment. The importance of surface mediation type effects to the adsorption of simple and complex gases is demonstrated. Coupled with the adsorption of simple gases is their projection area when used for surface area determination. The pressure dependence of a projection area is demonstrated for argon at 77 and 87.3 K. A simple model is used to account for the degree of graphitisation of a surface is demonstrated and used to account for the isosteric heat behaviour of non-graphitised carbon blacks. Turning from surfaces to porous solids, an alternative treatment of experiment data (either sub or super critical) is presented that avoids the ambiguity of excess amounts adsorbed. Using this method one is able to obtain pore size distributions and amounts adsorbed without relying on such things as helium expansion volumes. Since this type of method is usually applied to composite solids we also demonstrate the correct method for calculating the heat of adsorption using independent sets of simulations. The final topic covered in this paper is an example of the information that can be gained from the heat capacity of an adsorbed phase.

Keywords Molecular simulation · Carbon adsorbents · Surface interaction · Pore size distribution

Abbreviations

a_m	Molecular projection area nm^2
C_V	Heat capacity J/mol·K
g	Surface mediation factor –
$g(r)$	Radial distribution –
k_B	Boltzmann's constant J/K
k_{sf}	Binary interaction parameter –
L	Length of simulation box nm
m_p	Mass of adsorbent particles in cell kg
N_A	Avogadro's number mol^{-1}
N_{cell}	Total amount in adsorption cell mol
P	Pressure Pa
q	Partial charge on Coulombs site e
Q	Heat released J
q_{st}	Isosteric heat kJ/mol
r	Separation of interaction sites nm
S	Particle surface area m^2/kg
V	Volume m^3
z_0	Distance from surface at zero potential nm
ε	LJ well depth J
σ	LJ collision diameter nm
ε_0	Permittivity of a vacuum C^2/J·m
ρ_s	Surface density of carbon atoms nm^{-2}
ρ_b	Bulk density kmol/m^3
ρ	Average pore density kmol/m^3
Δ	Carbon layer separation nm
χ	Surface mediation damping constant –
Γ	Surface adsorption μmol/m^2
α	Volume of specific pore m^3/kg
φ	Interaction energy J

1 Introduction

Adsorption continues to be an active area of research. This is due to the wide range of industries that use adsorption as part of storage, separation and catalyst processes. Like any industrial process, the design and optimisation of industrial

G.R. Birkett · D.D. Do (✉)
School of Engineering, University of Queensland, St Lucia, QLD 4072, Australia
e-mail: duongd@cheque.uq.edu.au

adsorption processes relies upon the theoretical understanding of its underlying phenomena. Models used for adsorption have, by necessity, grown in complexity since the original coherent treatment of adsorption by Langmuir (1918). However it is now clear that there is no single classical theory for adsorption and their use is a currently a compromise between their ease of use for the engineering practitioner and their accuracy. The phenomenological approach to adsorption equilibria is being replaced by techniques that more directly take into account the underlying properties of the system. They include density functional theory, lattice gas theory and molecular simulations. The latter is the most widely applicable and currently the most widely applied. In principle if one can describe the molecular interactions of the system, one can calculate all the adsorption properties of the system of interest. This ideal is certainly far from being achieved due to limits in knowledge of molecular interactions and computer power. Nevertheless molecular simulations have become the predominant tool in the theoretical study of adsorption behaviour. In this paper we will present some aspects of the molecular simulation of adsorption that is of key concern to researchers interested in this area. These are the interaction potential of gases close to the surface, the molecular projection area and its consequence to surface area measurement, the effect of surface defects on the adsorption behaviour of graphite surfaces, a unambiguous technique for the comparison between simulation and experiment, the correct technique for the calculation of the heat of adsorption in a heterogeneous solid and the insight that can be gained from the analysis of adsorbed phase heat capacity.

2 Simulations and potential functions

The first application of the Monte Carlo method of integration to the calculation of fluid properties is attributed to Metropolis et al. (1953). Since that initial demonstration of the power of the technique, it has been applied to incredibly large array of systems of which adsorption represents a small sub set. Extensive reviews of the techniques used in Monte Carlo simulations and their history is presented in the texts of Allen and Tildesly (1987) and Frenkel and Smit (2002). The application of Monte Carlo simulations to adsorption systems has been covered by Nicholson and Parsonage (1982) and the points relevant to this paper are covered here.

2.1 Fluid potentials

All simulation studies considered in this chapter use single site or polyatomic molecules featuring dispersion sites and partial charges. The dispersive sites used in all models are Lennard Jones (LJ) sites. This is the most popular model for dispersive sites since there are a large number of parameters available in the literature for a range of fluids. The potential energy between two molecules is given by (1).

$$\varphi_{ij} = \sum_{a=1}^{A}\sum_{b=1}^{B}\frac{q_i^a q_j^b}{4\pi\varepsilon_0 r_{ij}^{ab}} + \sum_{c=1}^{C}\sum_{d=1}^{D}4\varepsilon_{ij}^{cd}\left[\left(\frac{\sigma_{ij}^{cd}}{r_{ij}^{cd}}\right)^{12} - \left(\frac{\sigma_{ij}^{cd}}{r_{ij}^{cd}}\right)^{6}\right] \quad (1)$$

where φ_{ij} is the interaction energy between fluid molecules i and j, A and B are the number of charges on the molecules i and j, respectively, C and D are the number of LJ sites on the molecules i and j, respectively, ε_0 is the permittivity of a vacuum, r_{ij}^{ab} is the separation between the charge a on molecule i and the charge b on molecule j having charges q_i^a and q_j^b, respectively and r_{ij}^{cd} is the separation between the LJ site c on molecule i and the LJ site d on molecule j with combined LJ well depth of ε_{ij}^{cd} and a combined LJ collision diameter of σ_{ij}^{cd} for the two sites. The values of ε_{ij}^{cd} and σ_{ij}^{cd} are given by Lorentz–Berthelot mixing rules in (2) and (3). Note the term $(1 - k_{sf})$ is used to approximate the deviation from the interaction predicted by the Lorentz–Berthelot mixing rule. So if it is assumed that the Lorentz–Berthelot mixing rule applies, $k_{sf} = 0$, and if there is some measurable deviation, k_{sf} can be adjusted to fit the relevant data.

$$\varepsilon_{ij}^{cd} = (1 - k_{sf})\sqrt{\varepsilon_i^c \varepsilon_j^d}, \quad (2)$$

$$\sigma_{ij}^{cd} = 0.5(\sigma_i^c + \sigma_j^d). \quad (3)$$

2.2 Surface potential

Monte Carlo simulations for bulk fluid replicate the, effectively, infinite nature of the fluid through the use of periodic boundary conditions, in three dimensions, and long range corrections to the truncated interaction potentials (Allen and Tildesley 1987). This is not possible for the simulation of slit type pores or surfaces since the fluid is no longer isotropic. A representation of a typical slit pore is given in Fig. 1 as the side projection of the pore. This shows that the pore is bound in the z-direction by two pore walls.

Although we show the graphite sheets as explicit atoms in Fig. 1, it is usual to assume that the carbon atoms can be treated as homogeneous and the attraction of an LJ atom to the surface is given by the famous Steele 10-4-3 potential (Steele 1973):

$$\varphi_{i,s} = \sum_{a=1}^{A} 2\pi\rho_s\varepsilon_{is}^a(\sigma_{is}^a)^2\Delta\left[\frac{2}{5}\left(\frac{\sigma_{is}^a}{z_i^a}\right)^{10} - \left(\frac{\sigma_{is}^a}{z_i^a}\right)^4 - \left(\frac{{\sigma_{is}^a}^4}{3\Delta(|z_i^a| + 0.61\Delta)^3}\right)\right] \quad (4)$$

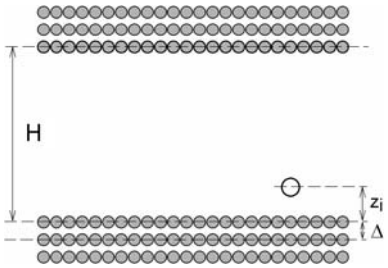

Fig. 1 Slit pore bound by several layers of graphite sheets

where $\varphi_{i,s}$ is the interaction between a molecule, i, and a uniform carbon surface, A is the number of LJ sites on molecule i, ρ_s (114 nm^{-3}) is the graphite's carbon density, Δ (0.3354 nm) is the separation distance between graphite layers, z_i^a is the shortest distance between LJ site a and the surface and ε_{is}^a and σ_{is}^a are the LJ well depth and collision diameter between site a and the surface calculated using (2) and (3), respectively. The LJ parameters for the Steele potential are $\sigma = 0.34$ nm, $\varepsilon/k_B = 28$ K.

2.3 Simulation methodology

Monte Carlo simulations were conducted using the grand canonical (GCMC) ensemble (Allen and Tildesley 1987). This is the natural choice for simulation studies since, for this ensemble, we specify the temperature, volume and chemical potential of the system. Given the equality of the bulk phase and adsorbed phase chemical potentials, we are able to relate the simulation isotherm to the adsorption isotherm through an appropriate equation of state.

For comparison with experiments conducted in the literature, the isosteric heat can be calculated from simulation. If it is assumed that the bulk phase gas is ideal and that the amount adsorbed in a simulation is much greater than the gas phase in the simulation, the isosteric heat can be calculated using (5) (Nicholson and Parsonage 1982).

$$q_{st} \cong \frac{\langle NU\rangle - \langle N\rangle\langle U\rangle}{\langle N^2\rangle - \langle N\rangle\langle N\rangle} + kT. \tag{5}$$

The first term in (5) can also be split into the different contributions of the system potential energy U. The three contributions to the potential energy are the fluid-fluid interactions, the fluid-surface interactions and the fluid-functional group interactions. Replacing U in (5) with one of these contributions to the potential, and discounting the second term, will give its contribution to the isosteric heat (Nicholson 1999). The heat capacity of the adsorbed phase can also be calculated. The configurational (i.e. ignoring kinetic and intramolecular contributions) component of the constant volume heat capacity, C_V^c, is calculated using (6) (Allen and Tildesley 1987).

$$C_V^c = \frac{(\langle U^2\rangle - \langle U\rangle\langle U\rangle) - \frac{(\langle UN\rangle - \langle U\rangle\langle N\rangle)^2}{\langle N^2\rangle - \langle N\rangle\langle N\rangle}}{\langle N\rangle k_b T^2}. \tag{6}$$

To investigate the origin of changes to the heat capacity, it is informative to calculate the contributions to the heat capacity from each component of the system interaction potential. The individual contributions to the heat capacity can be calculated using (Schofield 1966):

$$C_V^x = \frac{(\langle UU_x\rangle - \langle U\rangle\langle U_x\rangle) - \frac{(\langle UN\rangle - \langle U\rangle\langle N\rangle)(\langle U_xN\rangle - \langle U_x\rangle\langle N\rangle)}{\langle N^2\rangle - \langle N\rangle\langle N\rangle}}{\langle N\rangle k_B T^2}. \tag{7}$$

The final quantities we consider from simulation in this chapter are the density distribution functions. The local density at a distance z from the surface, commonly referred to as the z-distribution, is defined as:

$$\rho(z) = \frac{\langle \Delta N(z)\rangle}{L_x L_y \Delta z} \tag{8}$$

where $\Delta N(z)$ is the number of molecules whose centres of mass are in the segment whose boundaries are at z and $z + \Delta z$. It is also possible to define the z-distribution function for any of the sites on a molecule. The final distribution is the radial distribution (Allen and Tildesley 1987) function:

$$g(r) = \frac{V}{\langle N\rangle}\frac{\langle \Delta N(r)\rangle}{4\pi r^2 \Delta r} \tag{9}$$

where $\Delta N(r)$ is the number of interaction sites that are separated from another interaction site by a distance between r and $r + \Delta r$. In a bulk system, this function tends to a value of 1 at large values of r. This is not necessarily the case for adsorption system since they are not isotropic. However the radial distribution function is still informative for studying the association behaviour of fluids in adsorption systems.

3 Surface mediation

The simplest adsorption system that can be considered is that of a noble gas on graphitised thermal carbon black (GTCB). The most important example of this is argon adsorption on GTCB. Due to argon's simplicity and availability it is the next most popular fluid behind nitrogen for surface characterisation. It is only nitrogen's abundant availability that ensures it is the most popular fluid for use in surface characterisation. Extensive experimental adsorption data for argon on GTCB is available in the literature from a number of groups (Avgul and Kiselev 1970;

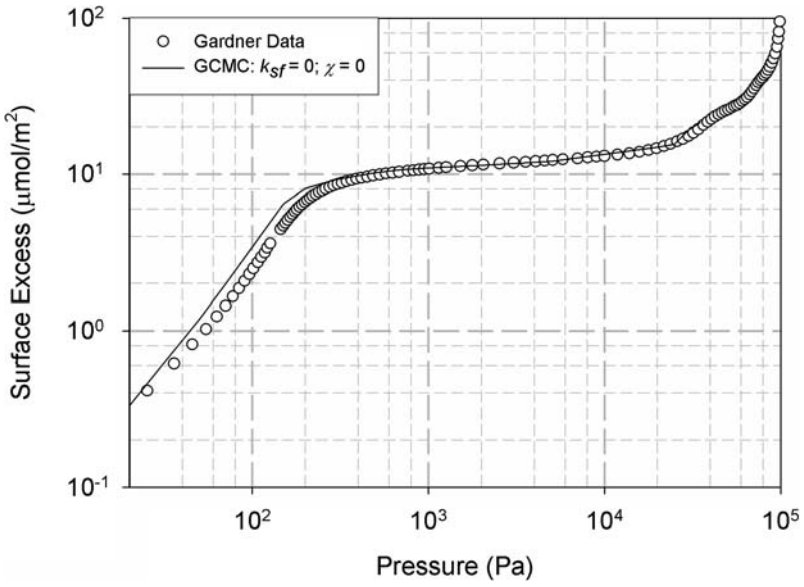

Fig. 2 Simulated adsorption isotherm (*solid line*) for the unmodified argon and solid potentials and the experimental data (*symbols*) for argon on GTCB at 87.3 K

Gardner et al. 2001; Olivier 1995). The data from Gardner et al. is the most recent and complete and we use it here for comparison with experiment. Using a Steele surface and the usual parameters for argon ($\sigma = 0.3405$ nm and $\varepsilon/k_B = 119.8$ K), the results of a GCMC simulation for argon at 87.3 K are presented in Fig. 2 (adapted from Do and Do 2007a) together with the experimental data of Gardner et al.

The simulation results show some significant disagreement with the experimental data. There is a small disagreement in the Henry's law region but the most noticeable difference is in the transition to monolayer coverage. Here the adsorption of argon is significantly over-estimated. The disagreement in the region of Henry's law is easy to resolve as either a short-coming in the Lorentz–Berthelot mixing rule or some small degree of heterogeneity on the surface. This can be accounted for by the use of the binary interaction parameter, k_{sf}, in (2) which can be set so that in the Henry's law region the results from simulation agree with experiment. The use of this parameter to fit the data in the Henry's law region has no impact on the deviation seen in the transition to monolayer coverage. To account for this it is necessary to introduce the concept of surface mediation. Surface mediation arises from the idea that fluid molecules close to the surface are distorted (compared to when they are in the isotropic environment of the bulk phase) and do not interact in the same way as they do in the bulk which is what is normally assumed for adsorption simulations. This concept is illustrated in Fig. 3 (Do et al. 2004).

The idea of surface mediation is not new and its effects on adsorbed molecules have been studied by a number of authors (Freeman 1958; McLachlan 1964; Sams 1965; Sams et al. 1962; Sinanoglu and Pitzer 1960). The reduction of the intermolecular potential energy when particles

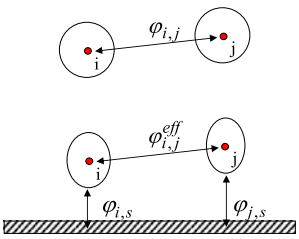

Fig. 3 Schematic diagram to illustrate the interaction between two fluid particles when they are away from the surface and when they are close to a solid surface

are close to the surface is thought to be due to having a dipole induced in the fluid molecules by the graphite surface (McLachlan 1964). Since the dipoles of two molecules close to the surface will be parallel the dipole of one particle will repel the dipole of the other. This in turn results in a reduction of the potential energy between the two particles. An effective treatment of this surface mediation has been handled in a number of ways such as adding additional terms to the LJ interaction equation. What we give here is a simple, functional equation to empirically deal with the effects of surface mediation on fluid-fluid interaction. The effective interaction of two fluid molecules under the influence of attraction by a surface is given by (10).

$$\varphi^{eff}_{i,j} = g\varphi_{i,j}, \tag{10a}$$

$$g = \exp\left(-\chi \frac{\varphi_{ij,s}}{k_B T}\right), \tag{10b}$$

$$\varphi_{ij,s} = \sqrt{\varphi_{i,s}\varphi_{j,s}} \tag{10c}$$

where g is the surface-mediation damping factor, $\varphi_{i,j}$ is the intermolecular interaction energy when two particles are in the bulk phase and are under no influence from the surface (i.e. calculated from (1)), χ is called the surface-mediated damping constant, $\varphi_{ij,s}$ is the geometric mean of the interaction of particles i and j with the surface and $\varphi_{i,s}$ is the

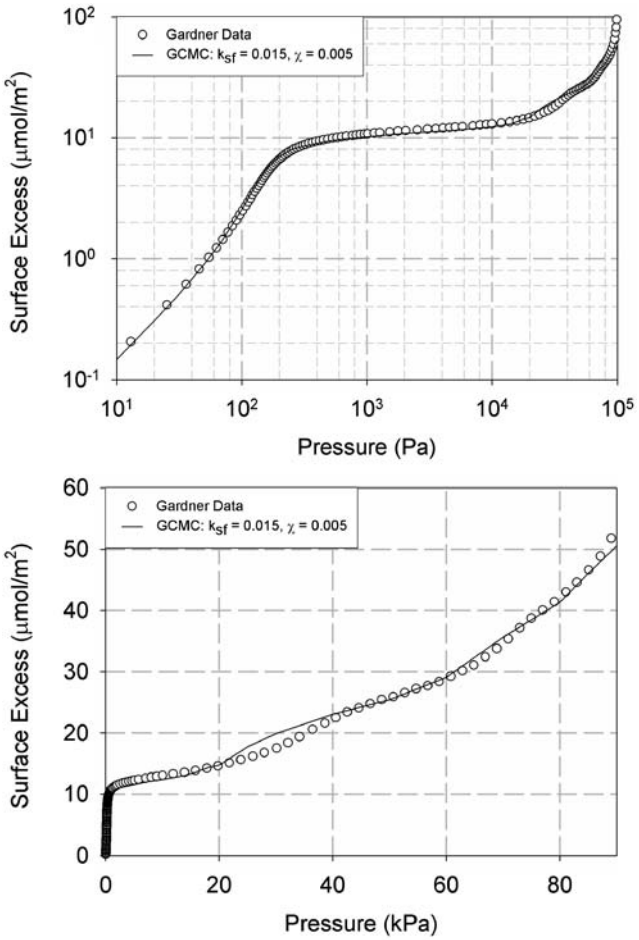

Fig. 4 Simulation results for argon (*solid line*) when using a surface mediation constant of 0.005 compared with experimental adsorption results (*empty circles*) on GTCB at 87.3 K on log-log and linear scales

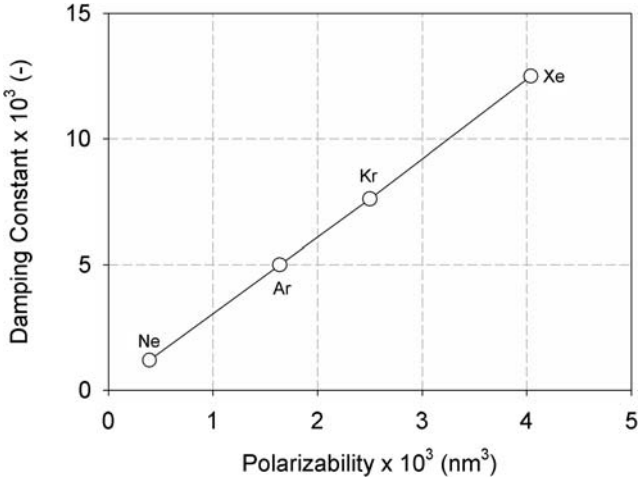

Fig. 5 Plot of the damping constant versus the polarizability of the fluid

interaction energy of molecule i with the surface calculated from (4). The form of (10b) and (10c) gives the properties of a maximum damping factor when both particles are close to the surface and a diminishing influence if one or both particles is far away from the surface. This is in line with the expectation that the surface mediation is a result of parallel induced dipoles, pointing in the same direction, for the two interacting fluid molecules.

Using this concept of surface mediation and using χ in (10b) as a tuning parameter, the fit between simulation and experimental data can be dramatically improved. With a damping constant of 0.005 the corresponding simulation results are presented in Fig. 4 (Do and Do 2005d) together with the experimental data. This figure shows a clearly superior fit between simulation and the experimental data compared to the case of no surface mediation in Fig. 2. For temperatures from 77 K to 130 K, the use of surface mediation was found to be necessary to correctly describe the adsorption of argon on GTCB (Do and Do 2005a). With the exception of 77 K (below the triple point of argon) the value of the damping constant required to fit the experimental data was found to be constant adding some weight the physical significance of surface mediation.

So whilst the use of surface mediation has been shown to be necessary for argon, it should also be applicable to the other noble gases and this has been shown to be the case for neon, xenon and krypton (Do and Do 2005b). For all the noble gases, the simulation isotherms without mediation always over-estimated the adsorption in the same manner as was seen for argon in Fig. 2. The introduction of surface mediation led to very good agreement with experiment for all noble gases. The temperature independence of the damping constant seen for argon was also observed for the other noble gases. These are strong indicator of the validity of surface mediation. Now we have mentioned that surface mediation may have its origin in the induction effects of the surface on the adsorbed particles. If this is the case, one would expect a relationship between the damping constant, χ, and the polarizability of the fluid in question. The relationship between the two is illustrated in Fig. 5 (adapted from Do and Do 2005b) to show a striking linear relationship between the two quantities. This is not absolute proof of the physical significance of surface mediation but is certainly a strong indicator of its validity.

As a further example of the importance of surface mediation, we consider the case of a complex molecule on GTCB, benzene. The various aspects of sub-critical benzene adsorption have been covered by Do and Do (2006a). From this study it was concluded the benzene model proposed by Wick et al. (2002) was the most suitable for studying adsorption on GTCB. The simulation results for this model on GTCB at 293 K with and without surface mediation are presented in Fig. 6 (Do and Do 2006a), together with experiment results of Isirikyan and Kiselev (1961). This shows that the simulation without surface mediation again over-estimates

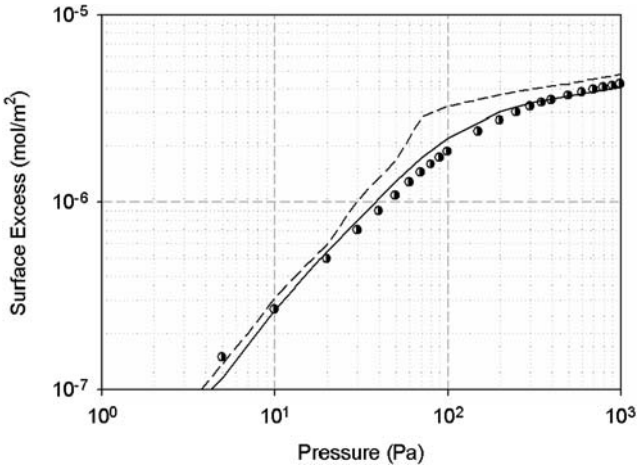

Fig. 6 Adsorption of isotherm of benzene on graphitised thermal carbon black at 293 K. *Filled symbols*: data of Isirikyan and Isirikyan and Kiselev (1961); *dashed line*: original model of WSKS; *solid line*: modified WSKS model with surface mediation

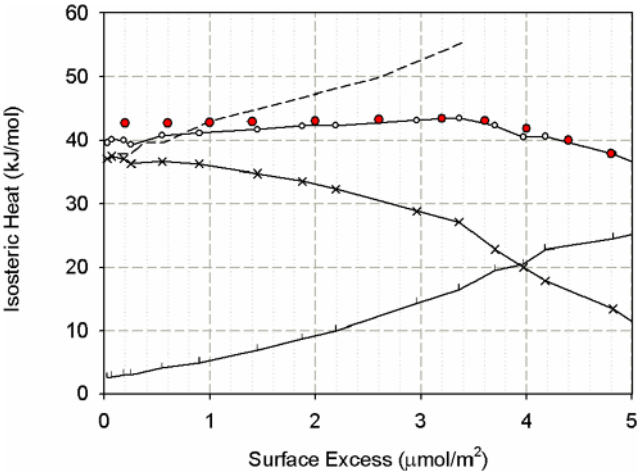

Fig. 7 Isosteric heat versus loading for benzene adsorption on GTCB at 293 K using the WSKS model. *Filled symbols* are the experimental data of Isirikyan and Kiselev while the *solid line with circle symbols* is the GCMC results using the WSKS with surface mediation. The *solid line with cross symbols* is the contribution of the solid-fluid interaction to the isosteric heat, while the *solid line with vertical bar* is the contribution of the fluid-fluid interaction

the adsorption. When surface mediation is used in the simulation, the agreement with experiment is greatly improved. The surface mediation constant for benzene on GTCB is also found to be independent of temperature as was seen for the noble gases. The importance of the surface mediation can also be demonstrated by the isosteric heat calculated from simulation shown in Fig. 7 (Do and Do 2006a) together with the experimental isosteric heat (Isirikyan and Kiselev 1961). This shows that without surface meditation (dashed line) the heat of adsorption is greatly over-predicted due to an over-estimation of fluid-fluid contribution to the isosteric heat. When surface mediation is used, the unusually flat sub-monolayer isosteric heat of benzene is extremely well produced by simulation. So here we have shown the value of surface mediation in the adsorption of noble gases and benzene. It has also been shown to be necessary to describe the adsorption of carbon tetrachloride (Do and Do 2006b) and nitrogen (Do and Do 2005c).

4 Projection area

An important application of the adsorption of gases on surfaces is for the measurement of surface area. This has been traditionally performed with nitrogen but there are some benefits to performing this task with argon. Regardless of which fluid is used, the accuracy of using adsorption to measure surface area relies upon two things, the successful description of isotherms and a correct estimation of the projection area of a molecule. Traditionally the projection area is taken from the liquid or solid densities of the fluid used. The equation used for the 2-dimensional projection area is that of Emmett and Brunauer (1937):

$$a_m = 1.091(\rho N_A)^{-2/3} \tag{11}$$

where a_m is the projection area per particle, ρ is the density of the bulk phase (liquid or solid) and N_A is Avogadro's number. For argon at 87.3 K this corresponds to projection areas of 0.1432 nm^2 and 0.1294 nm^2 using the liquid and solid density, respectively. At 77 K the (supercooled) liquid density gives a projection area of 0.138 nm^2 and the solid density is negligibly changed from 87.3 K. Experimental measurement tends to use one of these areas, either the liquid or solid based, when estimating the surface area of a solid. The voracity of doing this can be checked through the use of simulation. The projection area of a molecule in simulation can be measured by using the density of the first layer. Figure 8 (Birkett and Do 2007) shows the density profile of argon on GTCB from simulation. This is a typical profile for sub-critical gases that adsorb strongly to the surface and shows a clear definition between the first and second layers. If we define the first layer as extending to the mid point between the first and second layer (arrow in Fig. 8) it is possible to calculate the average number of molecules in this layer for the area of the simulation to give the projection area of the molecules in the first layer.

Using this calculation procedure, the projection area is calculated for the isotherms at 77 and 87.3 K. The results of this are plotted in Fig. 9 against the reduced pressure. Surface area determination is still performed predominantly with the BET equation and we will concern our discussion over the range of reduced pressure that this equation is normally applied, 0.05 to 0.3. It can be seen in Fig. 9 that the projection area at both 77 and 87.3 K changes significantly

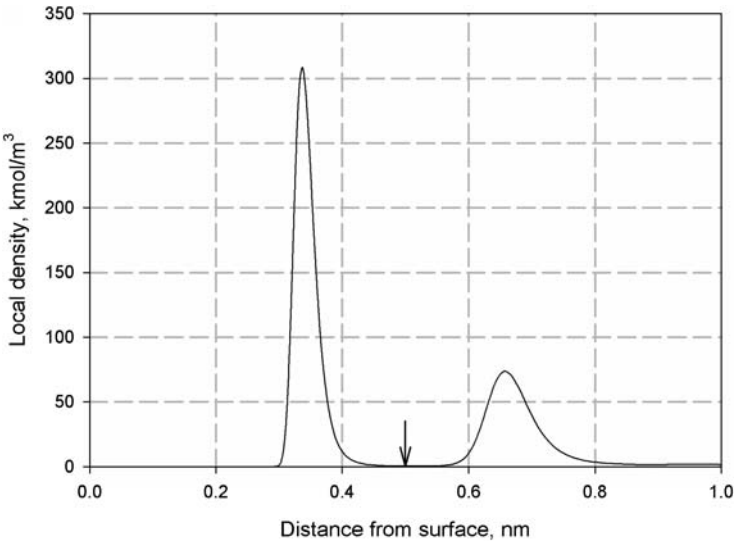

Fig. 8 Density of argon on a Steele surface at 87.3 K and 23.1 kPa as a function of its separation from the surface

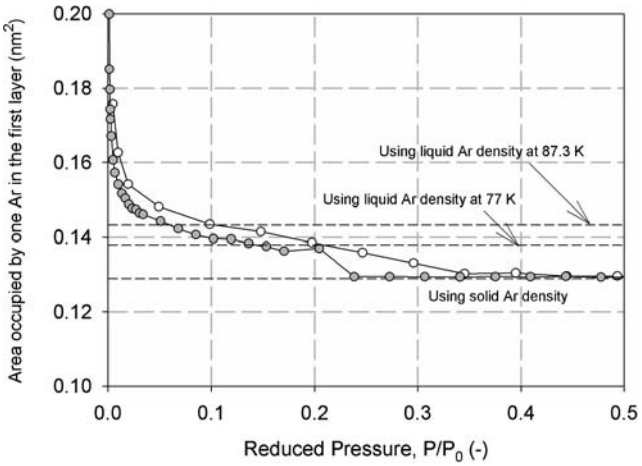

Fig. 9 Projection area of molecule in first layer versus reduced pressure for argon at 77 (*filled symbols*) and 87.3 K (*empty symbols*) from simulation on a Steele surface. *Horizontal dashed lines* refer to projection areas using (11) and densities as marked

over this range of pressure. The behaviour at 77 K is particularly interesting with projection are quite constant in the range of $P/P^{VAP} = 0.1$ to 0.2 and equal to the value calculated from (11) using the liquid density, 0.138 nm^2. When the reduced pressure is increased to 0.25, the first layer undergoes something similar to a liquid-solid transition and the projection area makes a step change to 0.1294 nm^2, the area predicted using the solid density. So whilst the agreement with (11) is good before and after the step change, it clearly demonstrates the pressure dependence of the projection area and the care that is required when choosing the range of data for surface area measurement. At 87.3 K the concept of projection area is even less clear with it decreasing with increasing pressure until a projection area corresponding to the solid state is reached at a reduced pressure of 0.35. For the BET range of pressure, the average value of the projection area is 0.14 nm^2 and this would be the value to use in this type of calculation. Projection areas of nitrogen at 77 K also exhibit similar behaviour to argon but will achieve projection areas even lower than that predicted by (11) using the solid density. This is due to the linear structure of nitrogen and its ability to pack perpendicular to the surface. Over the range of BET pressure, the average area of a nitrogen molecule is 0.155 nm^2 compared with the commonly used value of 0.162 nm^2(a difference of 4.5%).

5 Degrees of graphitisation

The surfaces considered in the section above have been fully graphitised surfaces with no defect in the graphite sheet. However there is no such thing as a perfectly graphitised surface (left hand side of Fig. 10), only surfaces that are so close we cannot discern the difference. Such closeness to graphitic perfection is not common amongst carbon blacks studied in the literature and the heterogeneous nature of the surface is detectable. Here we demonstrate a simple method of taking into account the degree of graphitisation (or non-graphitisation). This involves using a Steele surface as it usually modelled and placing an explicit graphite sheet upon it at the usual graphite sheet separation (0.3345 nm). If this graphite sheet is left as is (left hand side of Fig. 10), the adsorption behaviour is virtually identical to that of the Steele surface. Now to introduce defects to the surface, a carbon atom is chosen at random and all atoms within a certain distance, R_d, are removed as well. This is repeated until the desired degree of defect is achieved. The percentage of defect is defined as the ratio of atoms removed to atoms in a full sheet. So the non-graphitisation of the surface is defined by the percentage of defect and the defect radius. Figure 10

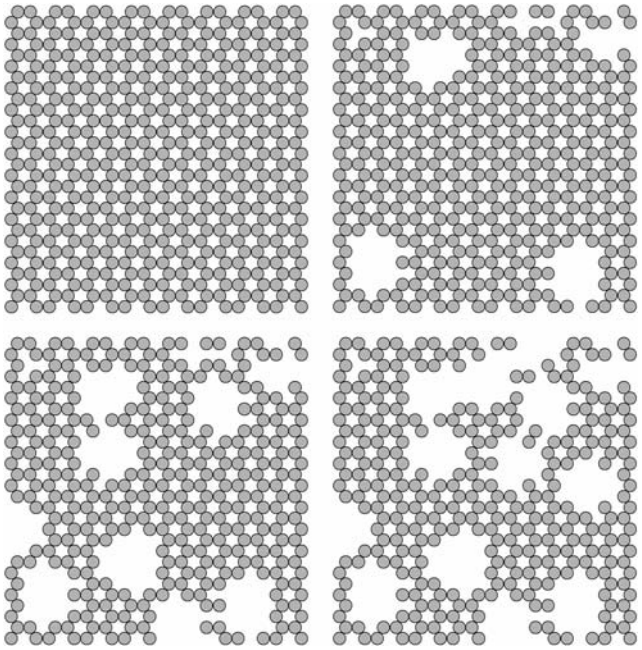

Fig. 10 The configuration of the top surface of non-graphitised carbon black. Clockwise from top left hand corner, the percentage of defect is 0, 10, 20, and 30%, and the effective defect radius is 0.284 nm

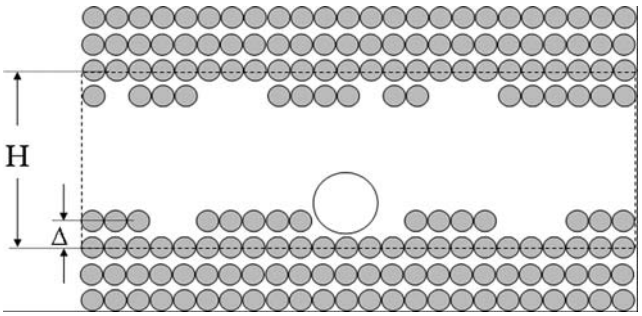

Fig. 11 Side projection of simulation box with non-graphitised surfaces

(Do and Do 2006c) shows the top view of a graphite sheet with a defect radius of 0.284 nm and defect percentages of 0, 10, 20 and 30% (from left to right). The side view of a simulation using the defected pore configuration is given in Fig. 11 (Do and Do 2006c).

The effect of the degree of graphitisation on the adsorption isotherms of argon is demonstrated in Fig. 12 (Do and Do 2006c) with adsorption on the surface depicted in Fig. 10. The surface with no defects results in the distinct layering behaviour that we have discussed in the previous surface mediation section for argon. However as the number of defects is increased, the transition to a monolayer coverage becomes less well defined due to the increasing disordered packing of the first layer. One can look at the monolayer transition of a defected surface and argue that it could be used to correct for the over-estimation from simulation at

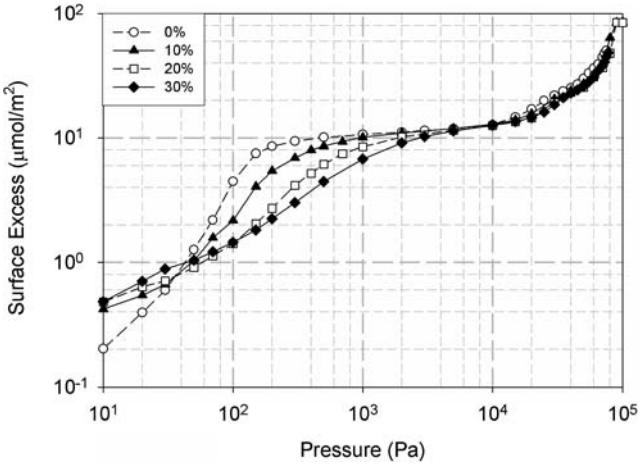

Fig. 12 Adsorption of argon at 87.3 K on non-graphitised carbon black with effective radius of two times the carbon-carbon bond length ($R_d = 0.284$ nm). The percentage of defect varies from 0 to 30%

the transition to monolayer coverage (Fig. 2) as an alternative to surface mediation (Fig. 4). This cannot be valid for highly graphitised carbon black where Henry's law behaviour is observed experimentally up to a pressure of about 30 Pa. All the non-graphitised carbon blacks (NGCBs) in Fig. 12 deviate from Henry's law behaviour at the lowest pressure considered of 10 Pa. This is contrast to what is seen from experiment for GTCB and cannot be a viable model for this surface.

Even though it is not an appropriate model for GTCB, the defected surface should be a good model for less well graphitised surfaces. To test this we use the experimental isosteric heat data of Polley et al. (1953) and Beebe and Young (1954) for a range of variously graphitised carbons starting with Spheron 6. The experimental results (symbols) are plotted in Fig. 13 (Do and Do 2006c) with the simulation results of surfaces with percentage defects as marked. The degree of defect in the solid should be inversely proportional to the treatment temperature and this is what results from matching simulation to experiment. The simulation results predict very well the features of decreasing graphitisation of higher zero loading isosteric heats and a more gradual transition to the second layer heat of adsorption. The least graphitised surface is that of the untreated Spheron 6 and its isosteric heat is remarkably well described by a simulation surface with 50% defects. This type of model can have application the simulation of porous carbons as well where purely slit pore geometries with Steele surfaces are found to be too restrictive to correctly predicting adsorption behaviour. This type of model offers considerable savings in computational expense compared with a fully atomistic model of a porous carbon.

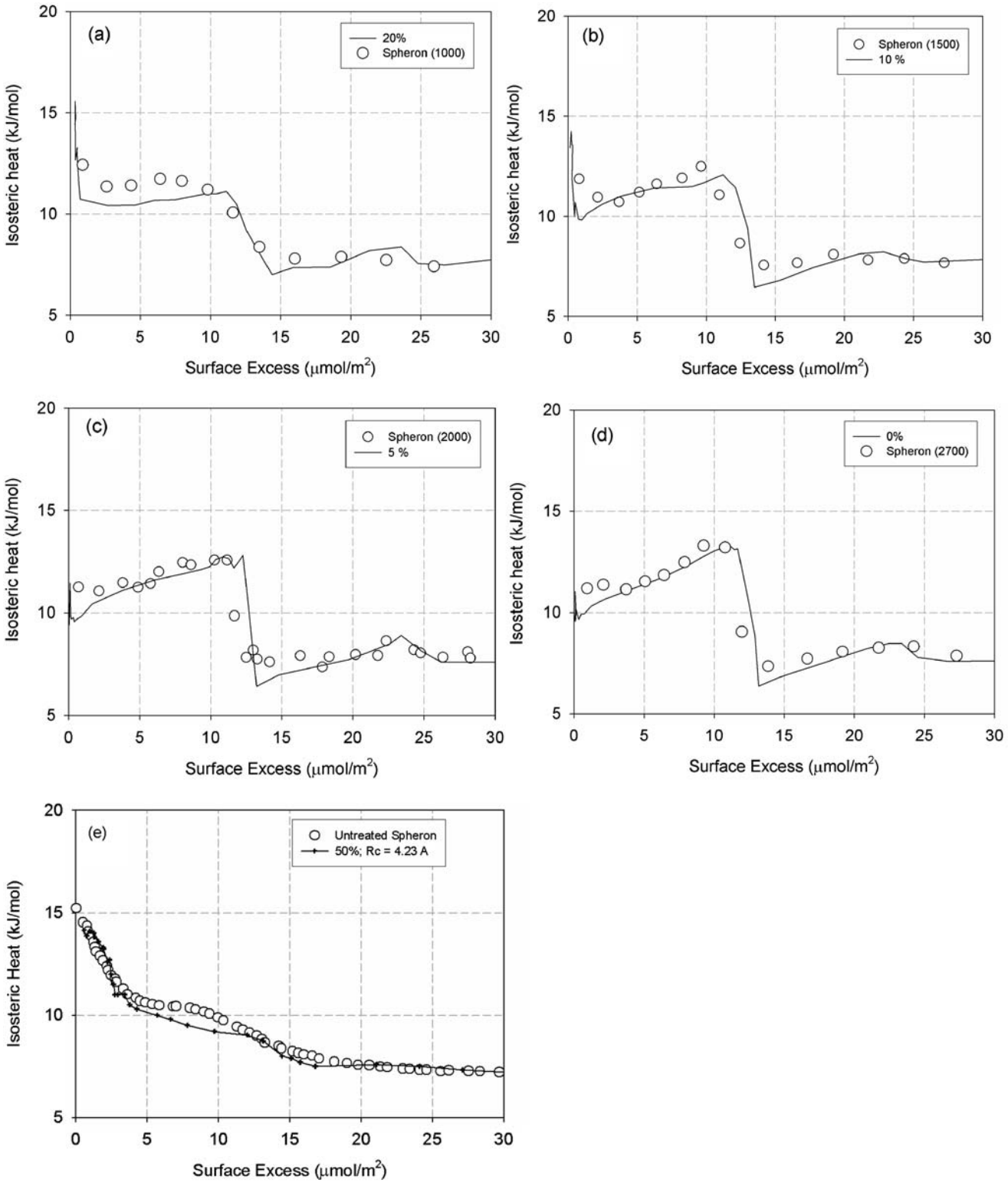

Fig. 13 Comparison between experimental isosteric heat data and GCMC simulation of adsorption of argon on surfaces of NGCB. (**a**) Spheron (1000); (**b**) Spheron (1500); (**c**) Spheron (2000); (**d**) Spheron (2700); (**e**) untreated Spheron

6 Unambiguous comparison with experiment

The results of volumetric adsorption experiments are traditionally collected as excess amounts adsorbed. The calculation of the excess amount adsorbed uses knowledge of the total amount in the adsorption cell, N_{cell}, the void volume in the adsorption cell and the bulk phase density. The total amount in the adsorption cell is easily and accurately calculated from the temperature and pressure of the reference dosing volume. The void volume is obtained using helium expansion at ambient temperatures. The void volume obtained from helium expansion, V^{He}, is subject to errors since the helium does adsorb to some degree on microporous solids and it can also access smaller pores than other types of fluids. This leads to an expected, but difficult to quantify, over-estimation of the void volume. Now to compare the excess amount adsorbed from experiment with simulation, it is required that the simulation isotherm be converted from absolute to excess amounts. This requires an estimation of the pore volume accessible to a fluid. For a slit pore (refer to Fig. 1) it is common to define an accessible pore width H' based upon the distance from the surface at which the fluid has an interaction energy of zero with the surface, z_0. It is then argued that the finite size of the molecule must be accounted for with resulting in the equation:

$$H' = H - 2z_0 + \sigma_{ff}. \tag{12}$$

Using this approach, the excess amount can be compared to simulation using (Birkett and Do 2006a):

$$\begin{aligned} &N_{cell}(P) - V^{He}\rho_b(P) \\ &\quad = m_p \int_0^{H*} [\rho'(P, H) - \rho_b(P)] dV^{acc} \\ &\qquad + m_p \Gamma^{ex}(P) \cdot S_{ext} \end{aligned} \tag{13}$$

where $\rho_b(P)$ is the density of the bulk phase at pressure P, m_p is the mass of adsorbent particles in the cell, $\rho'(P, H)$ is the average pore density based upon H' for a pore of characteristic width of H, V^{acc} is the accessible volume of the pore based upon H', $\Gamma^{ex}(P)$ is the surface excess for surface adsorption, and S_{ext} is the external surface area contributed by all pores having width greater than H^* (including the outside surface area of particles). Having already identified a problem with (13) with the use of V^{He}, there are also several difficulties in using (12). Firstly how is this defined for anything other than a regular geometry such as the defected pore in Fig. 11? Secondly, the term σ_{ff} is a superfluous artefact of intuition. It bears no consistency with bulk simulations (where we do not add σ_{ff} to the box length to calculate density) or simulation z-distributions which calculate the local density based upon only the volume corresponding to Δz in (8). Finally the distance z_0 is a function of pore topography (e.g. it can be affected by functional groups) and pressure where under the influence of fluid-fluid interactions, a fluid particle can approach the surface to a smaller distance than it otherwise would.

To circumvent this rash of ambiguity, we propose the use of only absolute quantities in the comparison between simulation and experiment. As mentioned above, the total amount in cell can be calculated accurately without ambiguity and it is this quantity we use to compare with simulation:

$$\begin{aligned} N_{cell}(P) = m_p \int_0^{H*} \rho(P, H)\, dV^{pore} + m_p \Gamma(P) \cdot S_{ext} \\ + V'' \rho_b(P) \end{aligned} \tag{14}$$

where $\rho(P, H)$ is the average density of the pore of size H at pressure P, V^{pore} is the characteristic volume of the pore and $\Gamma(P)$ is the absolute surface density of a finite sized surface simulation and V'' is the rest of the volume in the adsorption cell not associated with the solid, defined pore or the surface volume. Using (14) allows any definition of pore volume to be used and this allows it to be made the same as the volume of the simulation box (e.g. dotted line in Fig. 11). It also allows for the use of different pores of the same characteristic size but with different topologies (e.g. different degrees of surface defects). For a discrete number of simulations and pore sizes, the comparison between experiment and simulation using (14) allows the calculation of the pore size distribution. As an example, this has been completed using super critical methane at 273.15 K and up to 20 MPa (Birkett and Do 2006a). The pore size distribution derived from the experiment loading of the adsorption is given in Fig. 14 and the resulting fit with experiment data is given in Fig. 15.

It can be seen from Fig. 15 that the fit with experiment is very good and is arrived at without any assumptions made about the accessible volume of the system or the accessible volume of the pore structure. The term V'' in (14) is a fitting term like the pore volume and surface area when it comes to fitting the PSD. This volume will be a specific to that fluid. With the pores size distribution now obtained without unnecessary assumptions, it is now possible to calculate the properties of the solid using whatever assumptions are required. For example when a slit pore geometry is used for the simulations the surface area, S, can be calculated from:

$$S = S_{ext} + S_{\text{int}} = S_{ext} + \int_0^{H*} \frac{2f(H)}{H} dH. \tag{15}$$

Similarly the micropore volume, porosity, etc. can be calculated depending on the assumption one makes about the pores accessibility. The method we recommend for calculat-

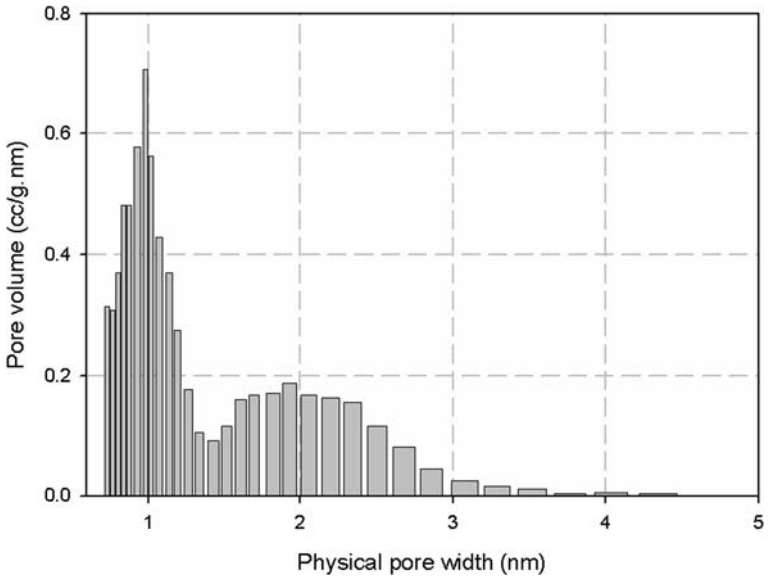

Fig. 14 Pore size distribution resulting from the fitting of experimental data at 273.15 K using the forward sequential optimization method and an initial PSD from N_2 adsorption

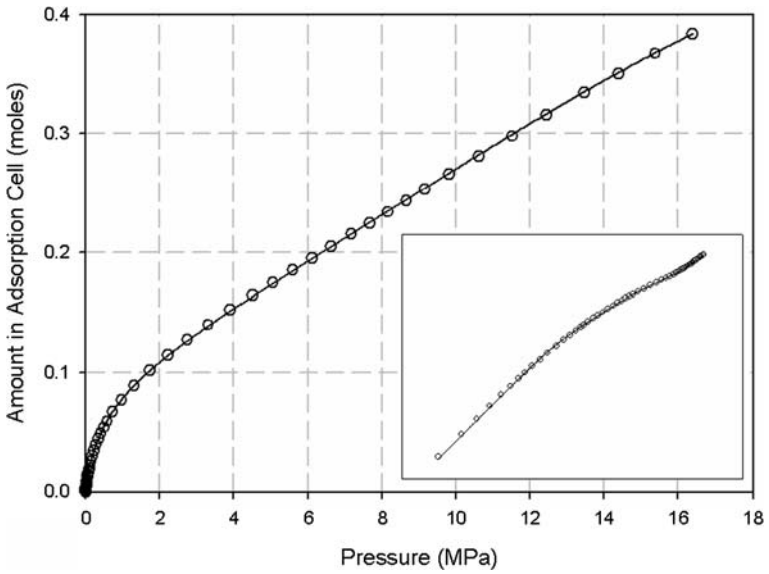

Fig. 15 Amount in adsorption cell at 273.15 K, from experiment (*empty circles*) and simulation (*line*) using the PSD in Fig. 14. *Inset* is the same plot in a log-log scale to show details at low pressure

ing the accessible volume of a pore is to calculate the volume in a pore where the interaction energy is zero or less. For a slit pore this can be calculated using (16). For a pore with a less regular geometry this can be calculated using a Monte Carlo type method (Do and Do 2006c). In this method particles are inserted into the simulation volume and the fraction of insertions that result in an interaction energy of zero or less with the surface is equal to the ratio of the accessible volume to the simulation volume. It would be possible to calculate this during a GCMC simulation with little additional computational expense.

$$H' = H - 2z_0. \tag{16}$$

7 Heat of adsorption for a heterogeneous solid

The calculation of isosteric heat for a heterogeneous solid can be obtained by either simulating the entire solid (i.e. as in all aspects of heterogeneity, not physical size) or by combining separate simulations. The combination of separate simulations is the common approach for calculating the properties of a heterogeneous carbon solid as was demonstrated in the previous section for isotherms. So for a collection of independent pores whose size is defined by their height, H_j, the isosteric heat has been traditionally calculated using (He and Seaton 2005; Nicholson 1999):

$$q_{st}^{porous}(P) = \frac{\sum_{j=1}^{N} \alpha_j \rho_j(P, H_j) q_{st,j}(P, H_j)}{\sum_{j=1}^{N} \alpha_j \rho_j(P, H_j)} \tag{17}$$

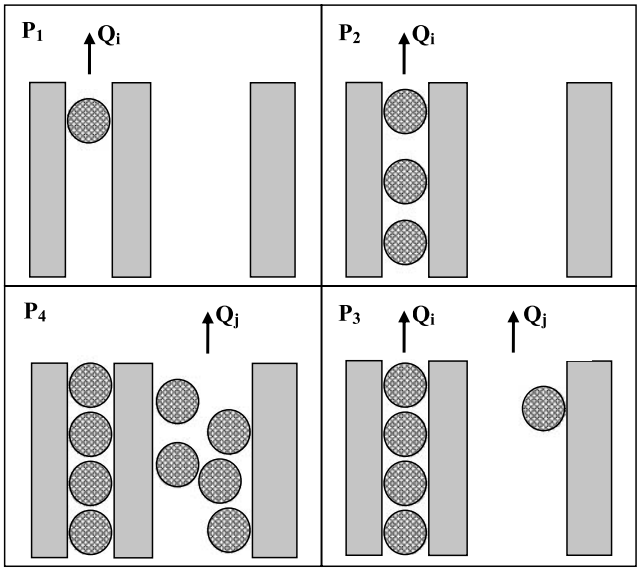

Fig. 16 Illustrative diagram of adsorption and heat generation (Q) of an idealised solid with two pores, i and j. From top left, pressure increases in the clockwise direction ($P_1 < P_2 < P_3 < P_4$)

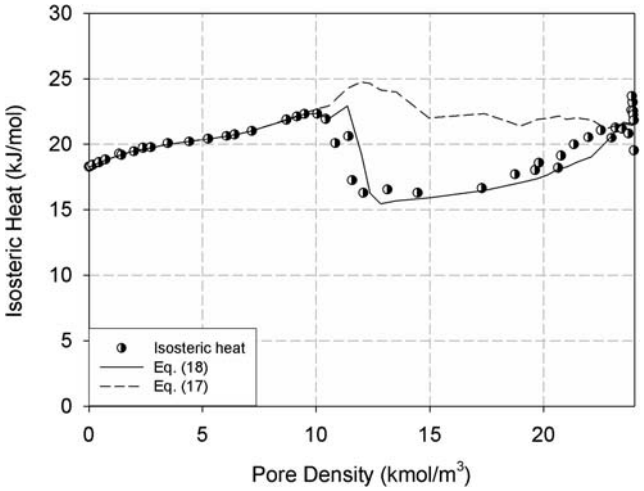

Fig. 17 Isosteric heat versus pore density, *symbols* are from the MC simulation of the two-pore system; the *solid line* is the calculated result from (18); the *dashed line* is the calculated result from (17)

where α_j is the specific volume of pores having a (characteristic) width H_j, ρ_j is the average density in this pore at the pressure P under consideration and $q_{st,j}$ is the isosteric heat of the same pore at the same pressure. Inspection of this formula shows that it is a weighted average of the isosteric heat using the amount adsorbed. This equation has been shown to be incorrect through several derivations and examples (Birkett and Do 2006b; Do and Do 2007b), one of which we discuss here. The correct equation for the isosteric heat for a heterogeneous solid is (Birkett and Do 2006b):

$$q_{st}(P) = \frac{\sum_{j=1}^{M} \alpha_j q_{st}(P, H_j) \frac{\partial \rho(P,H_j)}{\partial P}}{\sum_{j=1}^{M} \alpha_j \frac{\partial \rho(P,H_j)}{\partial P}} \tag{18}$$

where (17) is a weighted average to the amount adsorbed, (18) is a weighted average to the differential amount adsorbed. The error in (17) is that it gives weight to a pore that may be full and no longer adsorbing any fluid. This is illustrated in Fig. 16 (Birkett and Do 2006b) which shows a two pore system with pressure increasing from P_1 to P_4 and particles adsorbing and releasing heat at each increase in pressure. It is clear that in going from P_3 to P_4 that there is no adsorption in the smaller pore and that this pore does not contribute anything to the heat released from the two-pore solid. Equation (18) correctly describes this whereas (17) would still give a weight to the isosteric heat of the smaller pore.

To demonstrate the correct formula for the heat of adsorption in a porous solid (18), GCMC simulations are conducted on a simple two pore system similar to that in Fig. 16. The simulations are for argon at 87.3 K. For one set of GCMC simulations the two pores are modelled together using a layer of graphite sheet in the middle of a large pore to give two pores with a width of 0.7 and 0.8 nm (referred to as the 0.7, 0.8 nm pore). Two separate GCMC simulations are then run on slit pores of size 0.7 and 0.8 nm. The isosteric heats of these two pores are then combined using (17) and (18) to compare with the composite pore. The correct technique for combining isosteric heats of independent pores should agree with the results from the composite pore. The results of doing this are presented in Fig. 17 (Do and Do 2007b) where the heat of the composite pore (symbols) is plotted together with the result of combining the two separate simulations using (17) (dashed line) and (18) (solid line). It can be seen that the agreement between (18) and the composite pore is excellent whereas the calculation using (17) is in serious error. The fact that (17) is erroneous been demonstrated for a number of pore size combinations for both subcritical and super-critical conditions (Birkett and Do 2006b; Do and Do 2007b). Equation (18) should be equation used to combine isosteric heat data from independent simulation to when they are used to construct a heterogeneous solid.

8 Heat capacity

Having presented some of the aspects of adsorption isotherms and isosteric heats from molecular simulation, we now look at a rarely considered aspect of adsorption, the adsorbed phase heat capacity. To demonstrate some of the information about a surface that can be garnered from the heat capacity, we consider the adsorption of methanol on GTCB at 300 K. The model used for methanol is that of Chen et al. (Chen et al. 2001) with the methanol assumed to be rigid rather than flexible as proposed by its author. It consists of two LJ sites at the oxygen ($\sigma = 0.375$ nm, $\varepsilon/k_B = 98$ K and

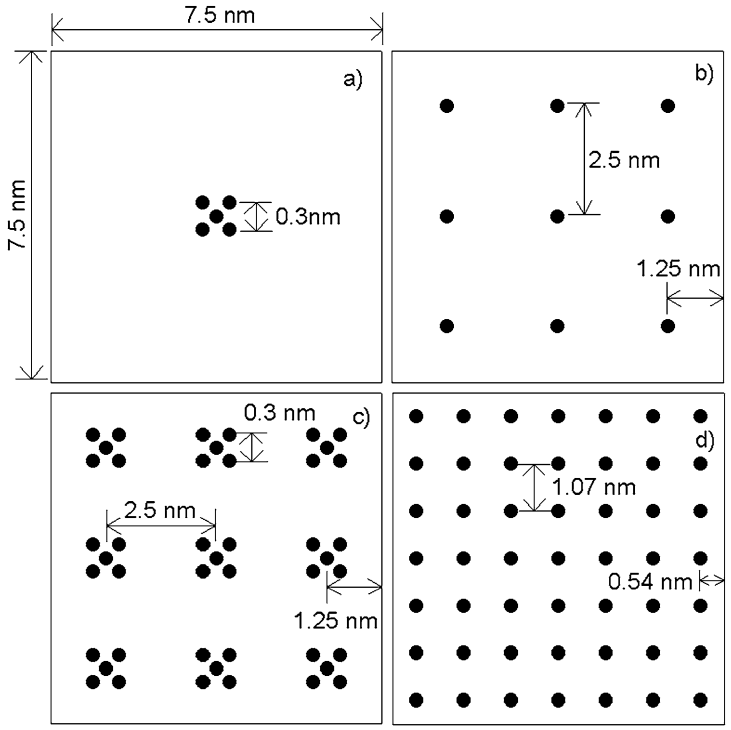

Fig. 18 Configurations of carbonyls (represented as *filled circles*) on the bottom plane of the pore (**a**) group of five carbonyls located at the centre of the pore wall, (**b**) nine evenly spaced carbonyls, (**c**) nine evenly spaced groups of five carbonyls and (**d**) 49 evenly spaced carbonyls. All configurations have the same box length of 7.5 nm

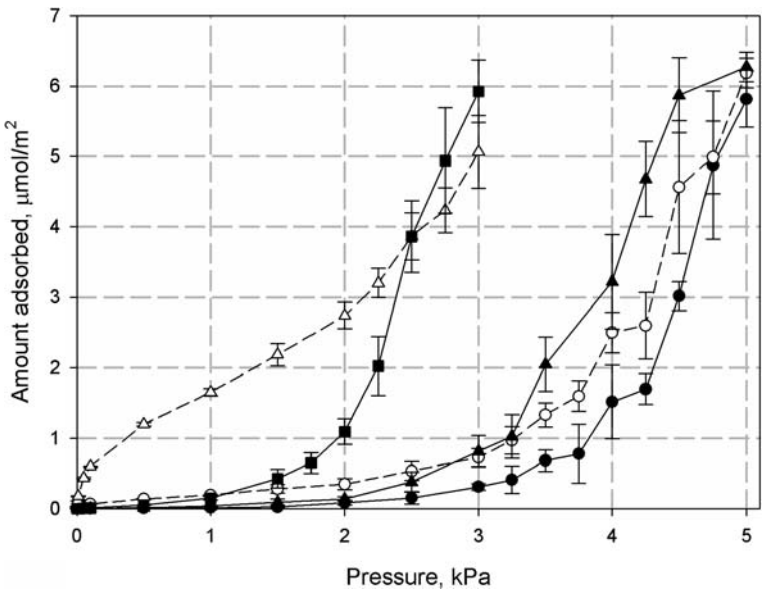

Fig. 19 Adsorption isotherms from simulation for methanol at 300 K on graphite (modelled using Steele potential) with no functional groups (*filled circles* and *solid line*), 5 grouped carbonyls (*empty circles* and *dashed line*), 9 evenly spaced carbonyls (*filled triangles* and *solid line*), 49 evenly spaced carbonyls (*filled squares* and *solid line*) and 9 evenly spaced groups of 5 carbonyls (*empty triangles* and *dashed line*). *Inset* is the same plot over a reduced pressure range to show detail. *Lines* are a guide for the eye only. Refer to Fig. 18 for diagram of carbonyl configurations

$q = -0.7$ e) and methyl group ($\sigma = 0.302$ nm, $\varepsilon/k_B = 93$ K and $q = +0.265$ e) and a partial charge at each and also at the hydroxyl hydrogen ($q = +0.435$ e). The three interaction sites are in the same plane and form an angle of 108.5°. This has been shown to be in good agreement with the experimental isotherms of methanol on GTCB. Now the adsorption of the methanol is considered on a Steele surface with various concentrations and configurations of carbonyls. The carbonyls are modelled as an LJ oxygen site with a partial charge ($\sigma = 0.296$ nm, $\varepsilon/k_B = 105.8$ K and $q = -0.5$ e) at a distance of 0.1233 nm from the surface and a partial charge located at the carbon surface ($q = +0.5$ e).

The results of the methanol simulations for these various surfaces in Fig. 18 are presented in Fig. 19 (Birkett and Do 2007). It can be seen that the addition of functional groups increases adsorption. At low pressure the greatest increase (per carbonyl) is due to the closely grouped carbons (Fig. 18a and 18c), whilst at higher pressure the isotherms

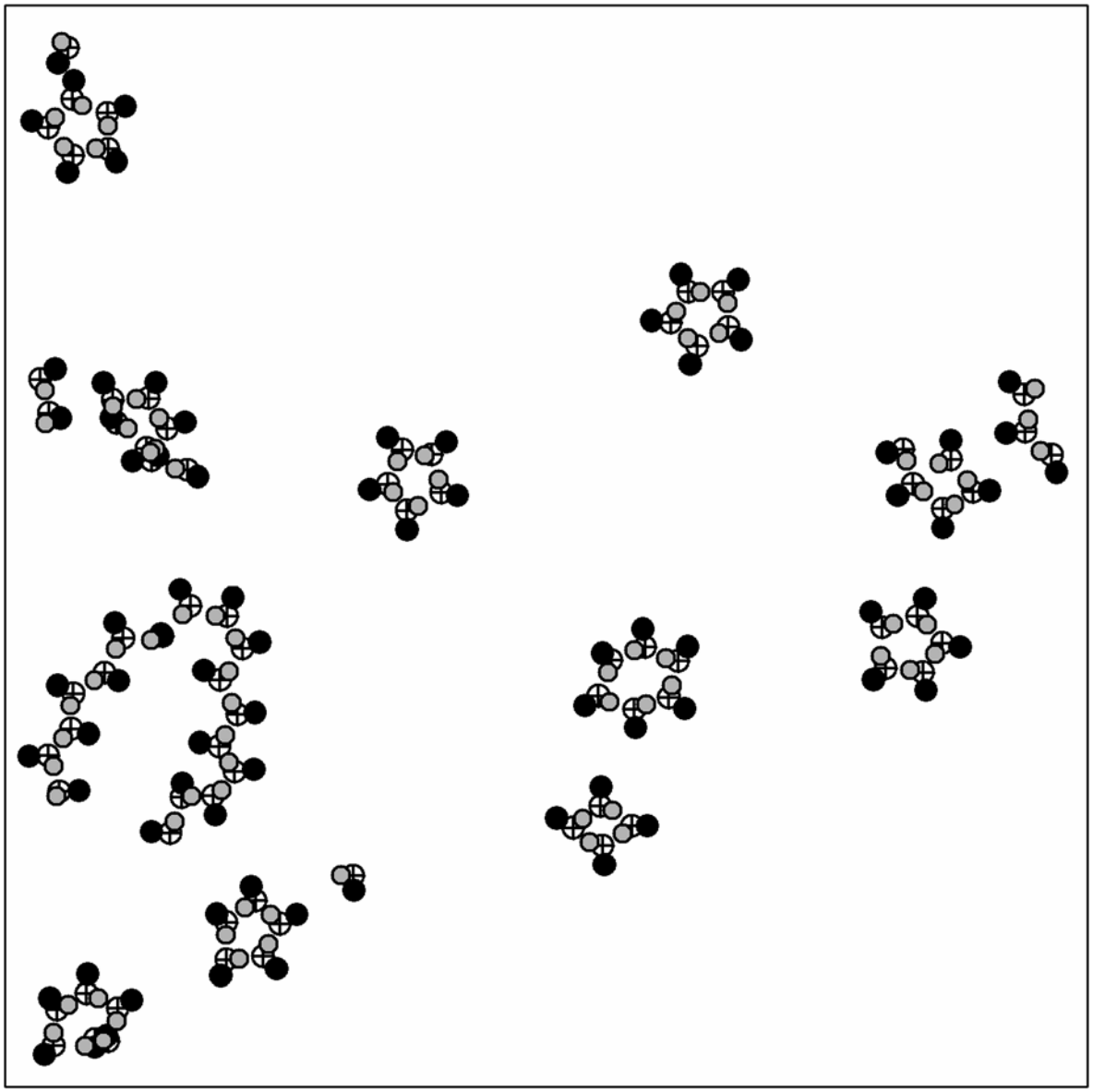

Fig. 20 Snapshot of methanol positions on bare carbon black for a simulation performed at 300 K and a reduced pressure of 0.27. Different groups are represented: CH_3 (*black*), O (*cross*) and H (*gray*)

of the evenly spread carbonyls (Fig. 18b and 18d) tend to be greater. The mechanism of adsorption for these systems has been shown to be one of adsorption at functional groups followed by two-dimensional clustering. The less attractive and the fewer the functional groups, the sooner this clustering begin. The clustering seen for methanol on the carbon surface is demonstrated in Fig. 20 (Birkett and Do 2006c) with a snapshot of methanol positions on a bare surface. This shows the small and disperse clusters that form at submonolayer coverage as typically tetramer or pentamer structures. The simulations of the bare surface and with a few functional groups (Fig. 18a and 18b) are all, within experimental error, in agreement with experiment. It is not possible to discern which surface is a better representation of the true surface from the isotherms alone.

Now we consider the heat capacity of the adsorbed phase calculated using (6). The heat capacities of the simulations presented in Fig. 19 are plotted in Fig. 21 (Birkett and Do 2007). This shows that the heat capacity of methanol has a clear maximum at low loading for all surface configurations except that corresponding to Fig. 18c (empty triangles) which has a much shallower peak at higher coverage. Now it is possible to investigate the source of the peaks in the heat capacity by decomposing the heat capacity to its contributions using (7). The results of this are plotted in Fig. 22 (Birkett and Do 2007) where it can be seen that the peaks

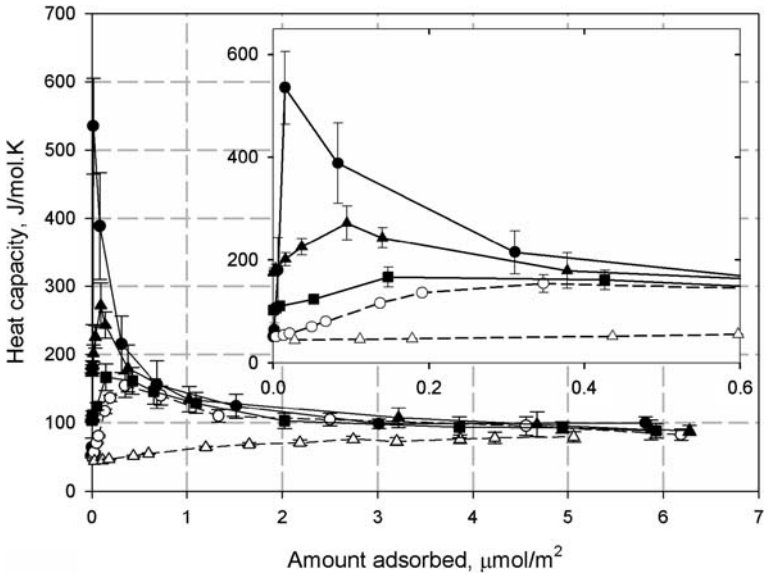

Fig. 21 Heat capacity from simulation for methanol at 300 K on graphite with various carbonyl configurations. *Inset* shows the details of the plot at low coverage. Symbols as per Fig. 19

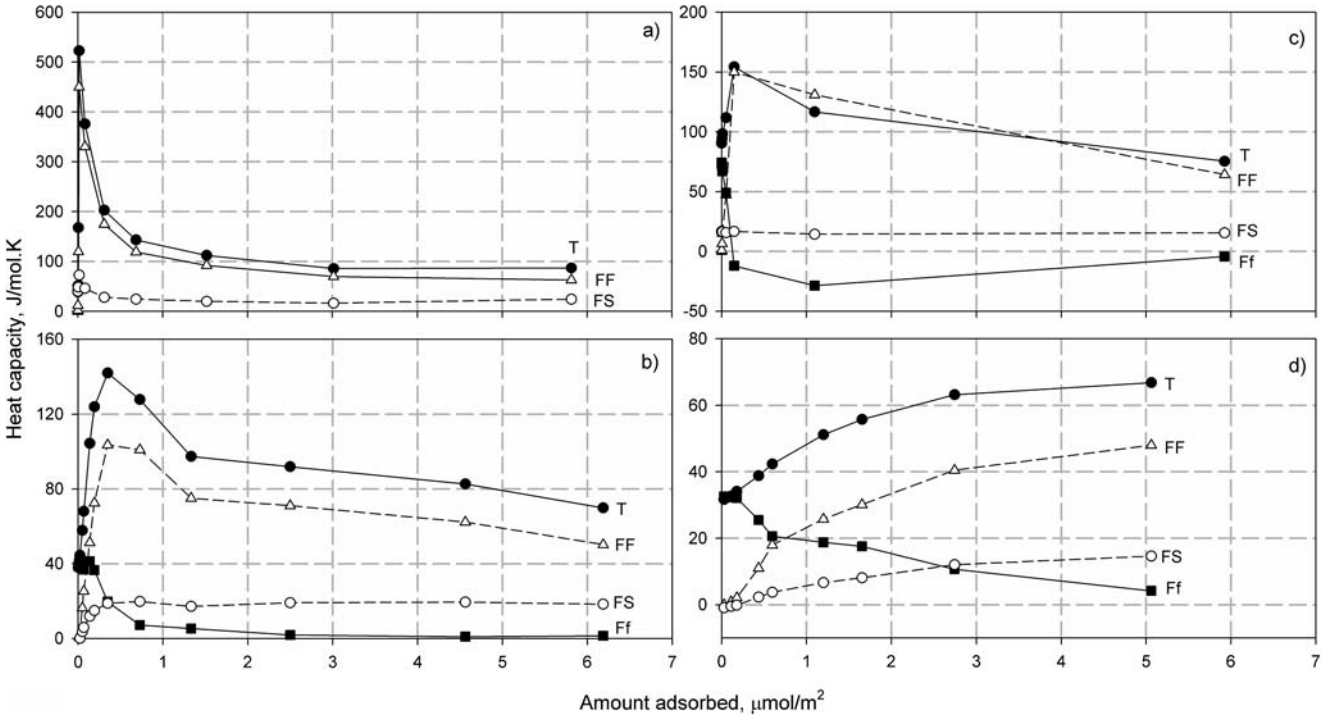

Fig. 22 Contributions to the heat capacity for methanol at 300 K on graphite with (**a**) no functional groups, (**b**) five carbonyls, (**c**) 49 evenly distributed carbonyls and (**d**) 9 groups of five carbonyls. Total energetic contribution (*T*, *filled circles*), fluid-fluid contributions (*FF*, *empty triangles*), fluid-surface contributions (*FS*, *empty circles*) and fluid-functional contributions (*Ff*, *filled squares*). *Lines* are a guide for the eye only. *X-axes* of all plots have the same scale but the scales of the *y-axes* are as marked

in the heat capacity for all surfaces (with peaks) is a peak in the fluid-fluid contributions (empty triangles) to the heat capacity. The decreasing peaks in the heat capacity with an increased number of carbonyls are due to a decrease in the peak in the fluid-fluid contributions.

The fluid-fluid contributions are due to the breaking of bonds with near neighbours. Using radial distributions, (9), it is possible to calculate the number of associated molecules per molecule in the simulation. For methanol, we define an associated molecule as having an O-H separation of less than 0.26 nm. The number of associated molecules has been calculated for methanol on a bare surface using NVT simulations at 300 and 304 K at the loadings presented in the same loadings as each data point in Fig. 21. The heat ca-

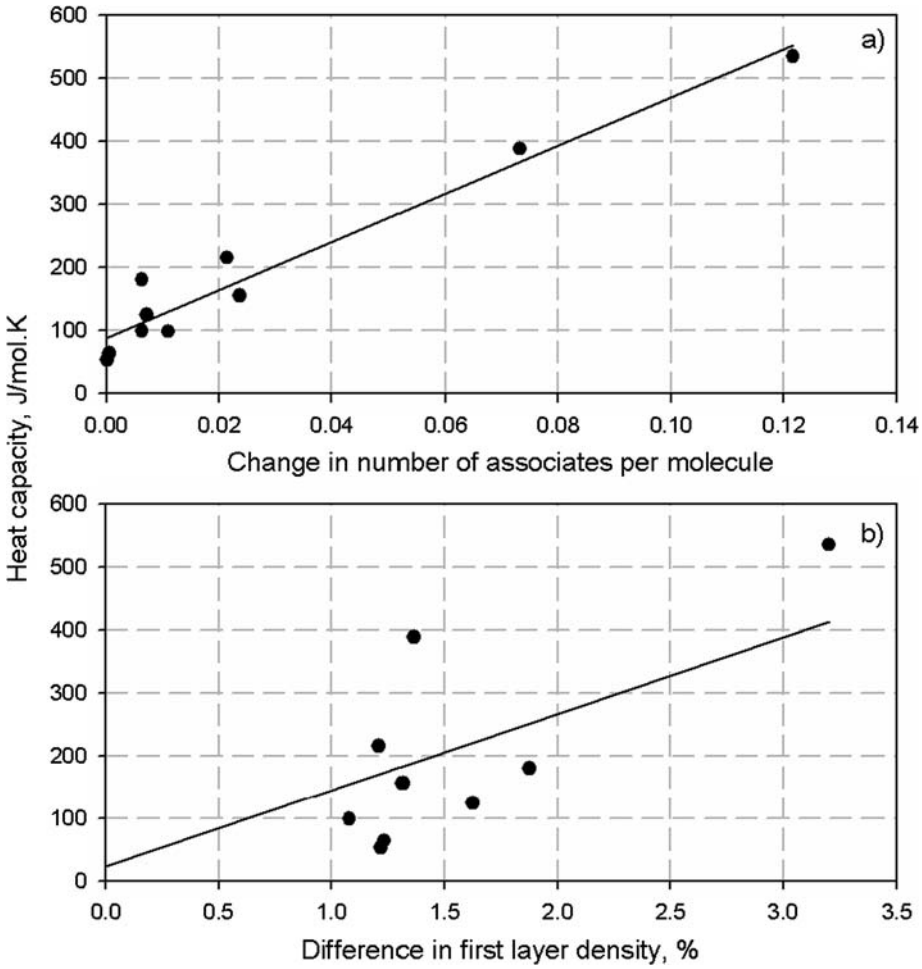

Fig. 23 Heat capacity versus the change in the number of associates per molecule (**a**) and the change in density of the fist layer (**b**) for methanol on a bare surface. The *solid lines* are linear regressions of plotted points

pacity is plotted as a function of the decrease in the number of associates, in heating from 300 to 304 K, in Fig. 23a (Birkett and Do 2007). Using the same NVT simulations it is possible to calculate the change in density in the first layer of methanol by performing a similar analysis to that done for projection area. The first layer for methanol is defined as those molecules whose methyl group is within 0.52 nm of the surface. The heat capacity is plotted as a function of the percentage decrease in first layer density, in heating from 300 to 304 K, in Fig. 23b. This shows that the heat capacity is most strongly related to the change in the number of associates with heating and is only weakly related to the change in the first layer density. This shows that the heat capacity for methanol, in sub-monolayer coverage, has its origins in the breaking of clusters (like those seen in Fig. 20) and not desorption from the surface.

The peak in the heat capacity for methanol presented here is also evident for ethanol (Birkett and Do 2006c) and to a lesser extent ammonia (Birkett and Do 2006c). The peak in the heat capacity of adsorbed alcohols has been observed in experiment (Berezin et al. 1969) on highly graphitised thermal carbon black. However the peak in the heat capacity seen from experiment is not as large as is predicted from simulation on a bare surface. So for agreement between experiment and simulation, there must be some functional groups present on even the most highly graphitised thermal carbon black. So where only small differences were seen between the isotherms of a bare surface and one lightly populated with functional groups, the heat capacity proves to be much more sensitive to the presence of these functional groups.

9 Conclusions

With this paper we have demonstrated a few of the more subtle aspects of molecular simulation as it is applied to adsorption. The topic of surface mediations shows the clear and discernable effect the surface has on the fluid-fluid interactions of adsorbing molecules. Since this has a strong effect on the adsorption of molecules such as argon and nitrogen this should be of concern to all who use these fluids as adsorption references for surface area measurement. In a similar manner the projection area of molecule in the

adsorbed phase is shown to be a function of pressure and the correct value must be used depending on the pressure range of data used for surface area measurement. A simple model for non-graphitised carbon blacks was presented and its applicability demonstrated against the isosteric heat data of variously graphitised carbon blacks. Comparison between simulation and experiment was considered in a general framework and formulation recommended using absolute quantities and absolute amounts adsorbed. Together with this the correct formulation for calculating the isosteric heat for a heterogeneous solid was presented with an example demonstrating the error in the currently used method. The final aspect discussed is the interesting behaviour of heat capacity data on surfaces and the potential for using it to characterise some aspect of the surface structure or chemistry.

Acknowledgements This research was made possible by the Australian Research Council whose support is gratefully acknowledged. Thanks also to the University of Queensland High Performance Computing facility for a generous allocation of computing time.

References

Allen, M.P., Tildesley, T.P.: Computer Simulation of Liquids. Clarendon, Oxford (1987)

Avgul, N.N., Kiselev, A.V.: Physical adsorption of gases and vapors on graphitised carbon blacks. Chem. Phys. Carbon **6**, 1–124 (1970)

Beebe, R.A., Young, D.M.: Heats of adsorption of argon on a series of carbon blacks graphitized at successively higher temperatures. J. Phys. Chem. **58**, 93–96 (1954)

Berezin, G.I., Kiselev, A.V., Kleshnina, I.V.: Heat capacities of alcohols adsorbed on graphitised carbon black. Russ. J. Phys. Chem. USSR **43**, 1657–1658 (1969)

Birkett, G., Do, D.D.: New method to determine PSD using supercritical adsorption: applied to methane adsorption in activated carbon. Langmuir **22**, 7622–7630 (2006a)

Birkett, G.R., Do, D.D.: Correct procedures for the calculation of heats of adsorption for heterogeneous adsorbents from molecular simulation. Langmuir **22**, 9976–9981 (2006b)

Birkett, G.R., Do, D.D.: Simulation study of methanol and ethanol adsorption on graphitised carbon black. Mol. Simul. **32**, 887–899 (2006c)

Birkett, G.R., Do, D.D.: On the heat capacity of adsorbed phases using molecular simulation. J. Chem. Phys. **126**, 064702 (2007)

Chen, B., Potoff, J.J., Siepmann, J.I.: Monte Carlo calculations for alcohols and their mixtures with alkanes. Transferable potentials for phase equilibria. 5. United-atom description of primary, secondary, and tertiary alcohols. J. Phys. Chem. B **105**, 3093–3104 (2001)

Do, D.D., Do, H.D.: Adsorption of argon on homogeneous graphitised thermal carbon black and heterogeneous carbon surface. J. Colloid Interface Sci. **287**, 452–460 (2005a)

Do, D.D., Do, H.D.: Effects of potential models in the vapor-liquid equilibria and adsorption of simple gases on graphitised thermal carbon black. Fluid Phase Equilib. **236**, 169–177 (2005b)

Do, D.D., Do, H.D.: Effects of surface heterogeneity on the adsorption of nitrogen on graphitised thermal carbon black. Mol. Simul. **31**, 651–659 (2005c)

Do, D.D., Do, H.D.: GCMC-surface area of carbonaceous materials with N2 and Ar adsorption as an alternative to the classical BET method. Carbon **43**, 2112–2121 (2005d)

Do, D.D., Do, H.D.: Adsorption of benzene on graphitised thermal carbon black: Reduction of the quadrupole moment in the adsorbed phase. Langmuir **22**, 1121–1128 (2006a)

Do, D.D., Do, H.D.: Adsorption of carbon tetrachloride on graphitised thermal carbon black and in slit graphitic pores: Five-site versus one-site potential models. J. Phys. Chem. B **110**, 9520–9528 (2006b)

Do, D.D., Do, H.D.: Modeling of adsorption on nongraphitized carbon surface: GCMC simulation studies and comparison with experimental data. J. Phys. Chem. B **110**, 17531–17538 (2006c)

Do, D.D., Do, H.D.: Effects of quadrupole moments of graphite surface on adsorption of simple gases on graphitised thermal carbon black. Colloids Surf. A Physicochem. Eng. Aspects **300**, 50–59 (2007a)

Do, D.D., Do, H.D.: Isotherm and heat of adsorption in porous solids with defective pores—Adsorption of argon and nitrogen at 77 K in Saran activated carbon. Mol. Simul. (2007b, in press)

Do, D.D., Do, H.D., Kaneko, K.: Effect of surface-perturbed intermolecular interaction on adsorption of simple gases on a graphitised carbon surface. Langmuir **20**, 7623–7629 (2004)

Emmett, P.H., Brunauer, S.: The use of low-temperature van der Waal adsorption isotherms in determining the surface area of iron synthetic ammonia catalysts. J. Am. Chem. Soc. **59**, 1553–1564 (1937)

Freeman, M.P.: The nature of the Vanderwaals interaction of gases and solids. 2. 3rd-order interaction. J. Phys. Chem. **62**, 729–732 (1958)

Frenkel, D., Smit, B.: Understanding Molecular Simulation. Academic Press, San Diego (2002)

Gardner, L., Kruk, M., Jaroniec, M.: Reference data for argon adsorption on graphitised and nongraphitized carbon blacks. J. Phys. Chem. B **105**, 12516–12523 (2001)

He, Y., Seaton, N.A.: Monte Carlo simulation and pore-size distribution analysis of the isosteric heat of adsorption of methane in activated carbon. Langmuir **21**, 8297–8301 (2005)

Isirikyan, A., Kiselev, A.V.: Absolute adsorption isotherms of vapors of nitrogen. Benzene and n-hexane, and heats of adsorption of benzene and n-hexane on graphitized carbon blacks. 1. Graphitized thermal blacks. J. Phys. Chem. **65**, 601–607 (1961)

Langmuir, I.: The adsorption of gases on plane surfaces of glass, mica and platinum. J. Am. Chem. Soc. **40**, 1361–1402 (1918)

McLachlan, A.D.: Van Der Waals forces between atom + surface. Mol. Phys. **7**, 381–388 (1964)

Metropolis, N., Rosenbluth, A.W., Rosenbluth, M.N., Teller, A.H., Teller, E.: Equation-of-state calculations by fast computing machines. J. Chem. Phys. **21**, 1087–1092 (1953)

Nicholson, D.: A simulation study of energetic and structural heterogeneity in slit-shaped pores. Langmuir **15**, 2508–2515 (1999)

Nicholson, D., Parsonage, N.G.: Computer Simulation and the Statistical Mechanics of Adsorption. Academic Press, London (1982)

Olivier, J.P.: Modeling physical adsorption on porous and nonporous solids using density functional theory. J. Porous Mater. **2**, 9–17 (1995)

Polley, M.H., Schaeffer, W.D., Smith, W.R.: Development of stepwise isotherms on carbon black surfaces. J. Phys. Chem. **57**, 469–471 (1953)

Sams, J.R.: Two-dimensional second virial coefficients of methane and tetradeuteromethane on graphitic carbon. J. Chem. Phys. **43**, 2243–2250 (1965)

Sams, J.R., Halsey, G.D., Constabaris, G.: Third- and fourth-order interactions of argon with a graphitised carbon black. J. Chem. Phys. **36**, 1334–1339 (1962)

Schofield, P.: Wavelength-dependent fluctuations in classical fluids. I. long wavelength limit. Proc. Phys. Soc. Lond. **88**, 149–170 (1966)

Sinanoglu, O., Pitzer, K.S.: Interactions between molecules adsorbed on a surface. J. Chem. Phys. **32**, 1279–1288 (1960)

Steele, W.A.: Physical interaction of gases with crystalline solids. I. Gas-solid energies and properties of isolated adsorbed atoms. Surf. Sci. **36**, 317–352 (1973)

Wick, C.D., Siepmann, J.I., Klotz, W.L., Schure, M.R.: Temperature effects on the retention of n-alkanes and arenes in helium-squalane gas-liquid chromatography—experiment and molecular simulation. J. Chromatogr. A **954**, 181–190 (2002)